Supporting Information

Dual-constrained assembly strategy of highly aligned two-dimensional montmorillonite membrane for efficient proton transport

Zhenlei Wang,[a,b,d] Lianqiu Huang,[a] Lingjie Zhang,*[a,b] Tingting Zhang,[c] Jianglin Yan,[a] Licai Chen,[a] Xiongrui Jiang,[a] Damiano Sarocchi,[d] Shaoxian Song,[a] Viridiana García Meza,[b] Mildred Quintana,[b] Yunliang Zhao*[a,e]

[a] *School of Resources and Environmental Engineering, Wuhan University of Technology, Wenzhi Street 34, Wuhan, Hubei 430070, China*

[b] *Facultad de Ciencias, Universidad Autonoma de San Luis Potosi, Av. Parque Chapultepec 1570, San Luis Potosi 78210, Mexico*

[c] *School of Chemical and Environmental Engineering, Wuhan Polytechnic University, Wuhan 430023, China*

[d] *Instituto de Geologia, Facultad de Ingeneria, Universidad Autonoma de San Luis Potosi, Av. Parque Chapultepec 1570, San Luis Potosi 78210, Mexico*

[e] *Wuhan Clayene Technology Co., Ltd., Tangxunhu North Road 36, Wuhan, Hubei 430223, China*

*Corresponding author:

E-mail address: zhanglj0515@163.com (L. Zhang), zyl286@whut.edu.cn (Y. Zhao)

Table of Contents

1. Supplementary texts

Text S1 Chemicals and Materials

Natural montmorillonite was obtained from Xinjiang, China. Poly (vinyl alcohol) (PVA, Mw 200000) and disodium 4-formyl-1,3-benzenedisulfonate (BADSA, 37%) were purchased from Sinopharm Chemical Reagent Co., Ltd. Sodium chloride (NaCl, ≥ 99%), potassium chloride (KCl, ≥ 99%), and hydrochloric acid (HCl, 37%) were purchased from Shanghai Aladdin Biochemical Technology Co., Ltd.

Text S2 Characterization

The thickness of the nanosheets and the surface roughness of the membranes were measured by atomic force microscopy (AFM, Multimode 8). The morphologies of nanosheets and membranes were obtained by scanning electron microscopy (SEM, Gemini SEM 300). Malvern Zetasizer ZetaNano (Malvern) was used to measure the zeta potential of the MMT colloidal dispersion. The X-ray Diffraction (XRD) pattern of membranes was performed by the powder X-ray diffraction (RU-200B/D/MAX-RB, Rigaku, Japan) with a Cu Kα radiation. The nanosheet stacking within membranes was investigated by a wide-angle X-ray scattering (WAXS, Xeuss 2.0) with Cu Kα radiation (λ=1.54189Å). Polarized optical microscopy (POM, Leica DM6 M) was used to observe the birefringence and dispersion degree of nanosheets and membranes. The tensile properties of membranes were measured on an Instron 5967 Tester. The X-ray Photoelectron Spectroscopy (XPS) was carried out by X-ray photoelectron spectroscopy ESCALAB 250Xi, Thermo Fisher Scientific, USA) for exploring the inner chemistry of nanosheets and membranes. The chemical composition and molecular structure of SPVA were analyzed by Fourier transform infrared spectroscopy (FTIR, Nicolet 6700,

Thermofisher) and nuclear magnetic resonance (NMR, Bruker AVANCE III spectrometer).

Text S3 Preparation of Sulfonated polyvinyl alcohol (SPVA)

The SPVA was prepared via an acid-catalyzed reaction between PVA and BADSA.[1] The specific experimental procedure was as follows: BADSA (50 mmol) and HCl solution (10 mL, 1 mol L^{-1}) were added to aqueous PVA solution (100 mL, 5 wt%). The reaction was carried out in a water bath at 60 ℃ for 96 h. The product was then precipitated in excess ethanol. Finally, the resulting white precipitates were washed three times with anhydrous ethanol and dried in a blast oven at 60 ℃ for 36 h to obtain SPVA.

Text S4 Liquid nitrogen transient freeze-drying treatment

The MMT and SMMT nanosheet dispersions were magnetically stirred for 24h, respectively, to ensure uniform dispersion. The uniformly dispersed nanosheets were left to stand for 48 h, then poured onto aluminum disks, which were subsequently immersed in liquid nitrogen for transient freezing. Further, the frozen samples were freeze-dried for 24 h (-60 ℃, 0.011 mBar). Finally, the suspension states of MMT and SMMT nanosheets were observed by scanning electron microscopy (SEM).

Text S5 Orientation factor calculation

The orientation factor (*f*) was used to describe the orientation degree of the nanosheets within the membranes. It's value ranges from 0 to 1, with larger values resulting in more consistent relative orientations.[2] The Herman's orientation function was used to fit the azimuthal profile:

$$f = \frac{1}{2}(3\langle\cos^2\theta - 1\rangle) \quad \text{(S1)}$$

$$\langle \cos^2\theta \rangle = \frac{\int_0^{\pi/2} I(\theta) \cos^2\theta \sin\theta \, d\theta}{\int_0^{\pi/2} I(\theta) \sin\theta \, d\theta} \quad \text{(S2)}$$

where $I(\theta)$ refers the azimuthal dependence of the X-ray scattered intensity.

Text S6 Ion exchange capacity determination

The ion exchange capacity (IEC) value of membranes was measured using a titration method.[3] Briefly, the dried membranes (0.2 g) were immersed in NaCl solution (0.1 g mL^{-1}, 20 mL) and stirred for 24 h to allow complete replacement of Na^+ and H^+. The solution was then titrated with 0.01 M NaOH solution, with phenolphthalein as an indicator. The IEC value (mmol g^{-1}) was defined as:

$$IEC = \frac{0.01 \times V_{NaOH}}{W_{dry}} \times 1000 \quad \text{(S3)}$$

where V_{NaOH} (L) is the consumed volume of the NaOH solution; W_{dry} (g) is the weight of the membrane.

Text S7 Degree of sulfonation determination

The sulfonation degree (Ds) of the prepared SPVA is accurately determined by ^{1}H NMR.[4] Specifically, the Ds is calculated based on the ratio of the integral areas of the methyl hydrogen atoms (Hp) and methylene hydrogen atoms (Hn) connected to the benzene ring on the hexagonal ring in the PVA chain repeat units, which can be calculated using the following equation.

$$Ds = \frac{2A_{(Hp)}}{A_{(Hn)}} \times 100\% \quad \text{(S4)}$$

Text S8 Theoretical calculations

The density functional theory (DFT) calculations were carried out by the Materials Studio

8.0 software. The exchange-correlation interactions were described by the Perdew-Burke-Ernzerhof generalized gradient approximation (GGA-PBE) for structure optimization to minimize the energy. The cut-off energy was set to 580 eV and the k-point mesh with a size of 3 × 1 × 1 grid was used. The convergence criteria for energy, displacement, and force were 1×10^{-5} eV/atom, 0.001 Å, and 0.005 eV/Å, respectively. The binding energy (E_b) were calculated by:

$$E_b = = E_{total} - E_{slab} - E_M \quad \text{(S5)}$$

where E_{total} indicates the total energy of the system; E_{slab} and E_M are the energies of individual SO_3^- and M ions, respectively.

2. Supplementary figures

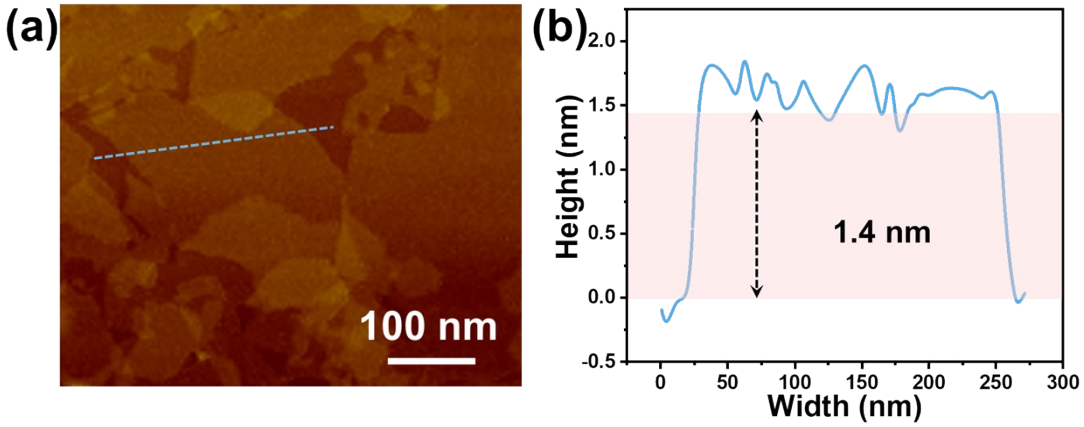

Figure S1. The atomic force microscopy (AFM) image and corresponding monocrystal diameter of the typical MMT nanosheets.

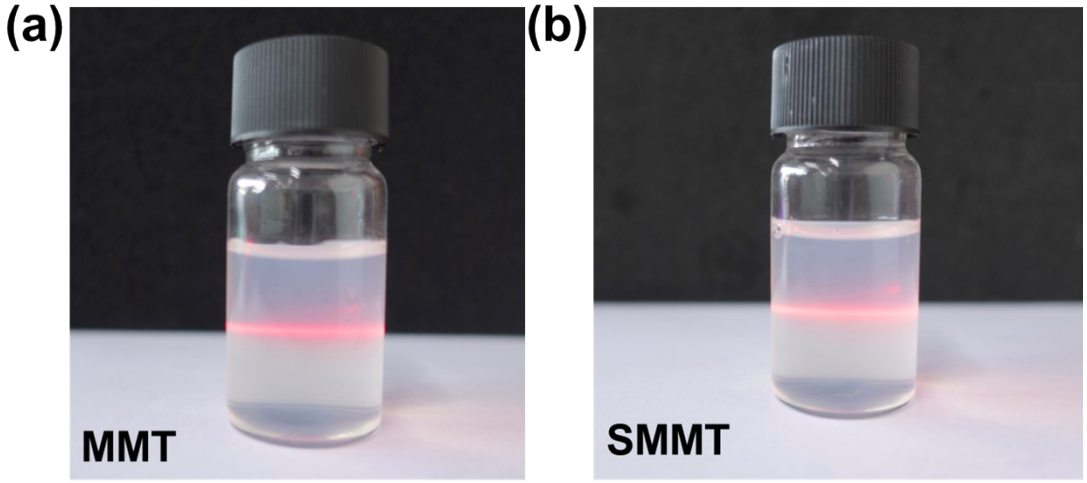

Figure S2. Photographs of the montmorillonite nanosheets (a) before and (b) after SPVA modification under a red laser beam.

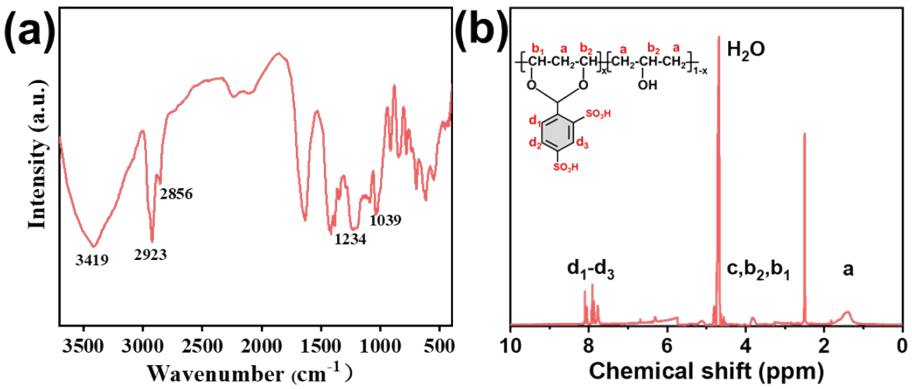

Figure S3. (a) FTIR and (b) ^{1}H NMR spectra of SPVA.

Note: The absorption peaks at 3419, 2923 and 2856 cm^{-1} were attributed to the asymmetric and symmetric stretching vibration peaks of -CH_2 and -OH in SPVA, and the characteristic peaks of S=O stretching vibration appeared at 1123 and 1039 cm^{-1}, and the infrared results indicated the successful synthesis of SPVA. The chemical composition of SPVA was further confirmed by ^{1}H NMR spectroscopy, where peaks between 7.7 and 8.2 ppm corresponded to the signals (d_1-d_3) of aromatic protons in BADSA. Further, the sulfonation degree (Ds) of SPVA is 17.2% according to the Equation S4, indicating that the prepared SPVA has a high sulfonation degree.

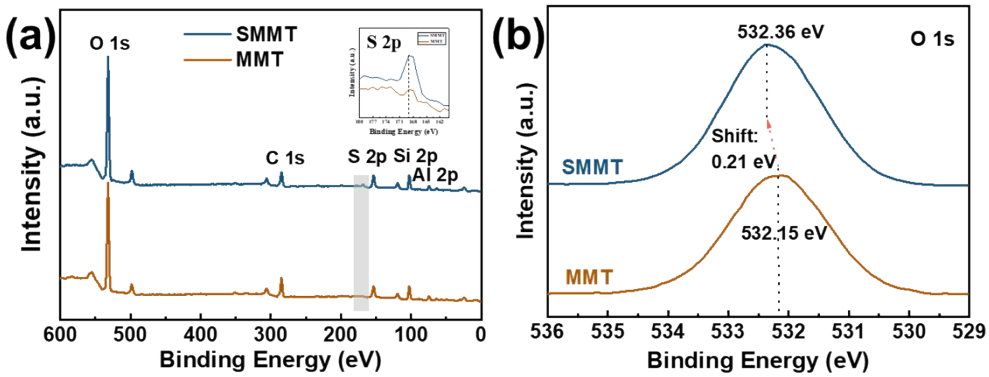

Figure S4. XPS spectra of full spectra (a) and O 1s (b) for MMT nanosheets before and after SPVA modification.

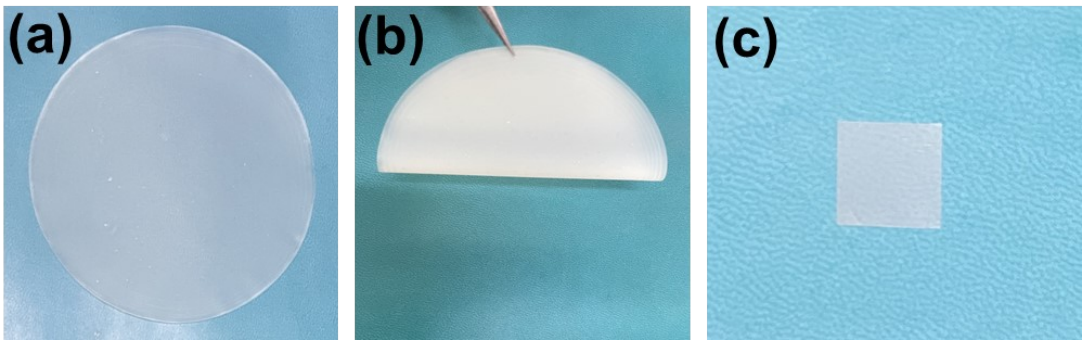

Figure S5. Photographs of the self-supporting SMMT membrane.

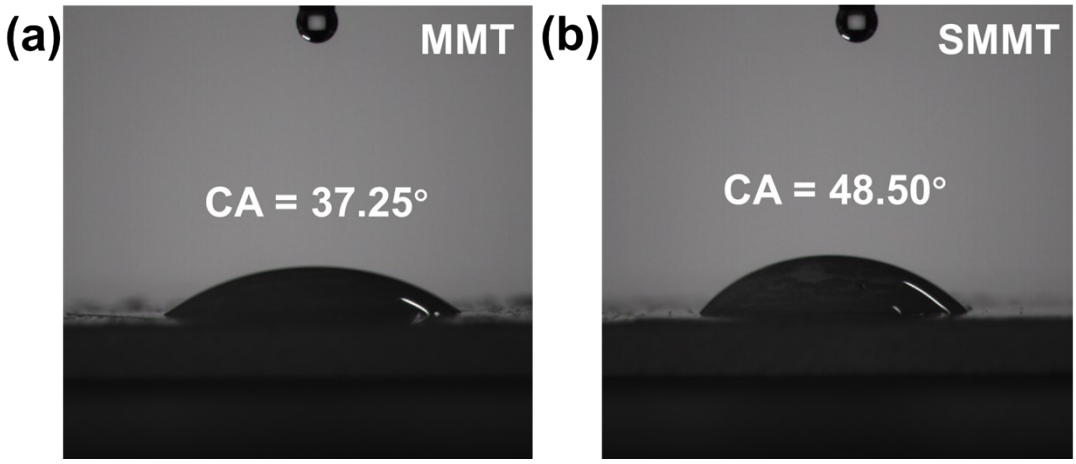

Figure S6. Water contact angle images of (a) MMT membrane and (b) SMMT membrane.

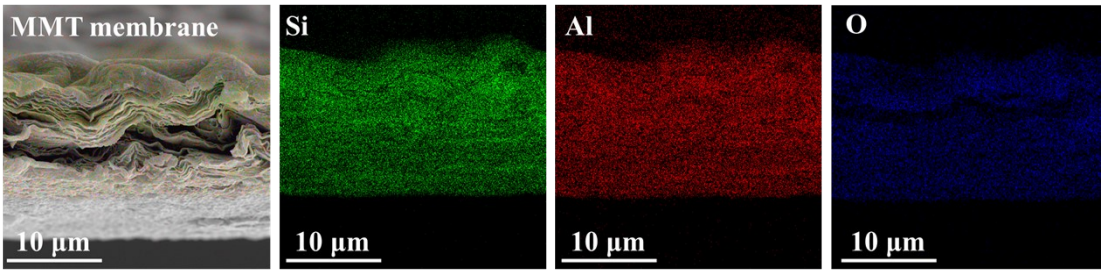

Figure S7. The EDS mapping of the cross section of the MMT membrane.

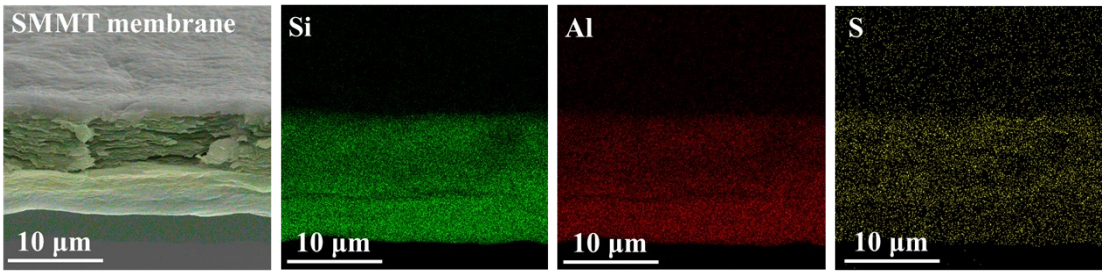

Figure S8. The EDS mapping of the cross section of the SMMT membrane.

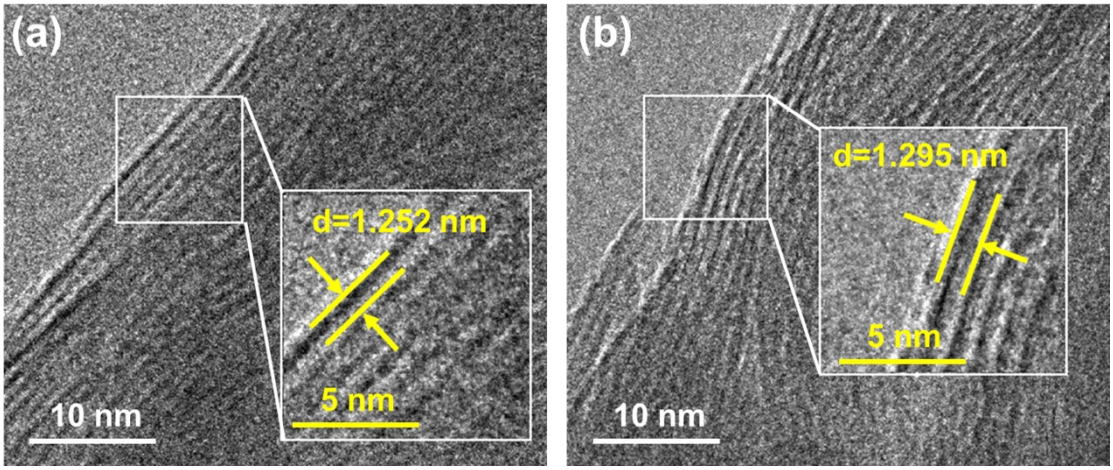

Figure S9. TEM images of (a) MMT and (b) SMMT membranes.

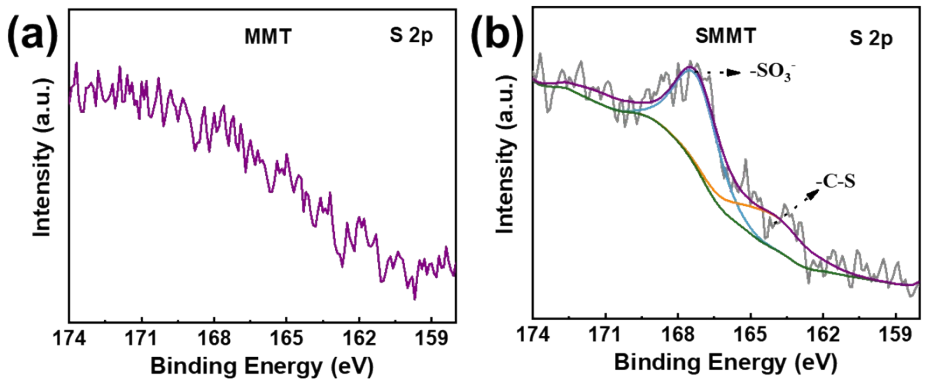

Figure S10. S 2p core level XPS spectra for (a) MMT and (b) SMMT membranes.

Note: The chemical changes in the SPVA-modified MMT membranes were further revealed by XPS analysis, where characteristic peaks of sulfonic acid groups (including $-SO_3^-$ and -C-S bond) appeared in the S 2p XPS spectral analysis of SMMT, whereas this functional group was clearly absent in MMT.

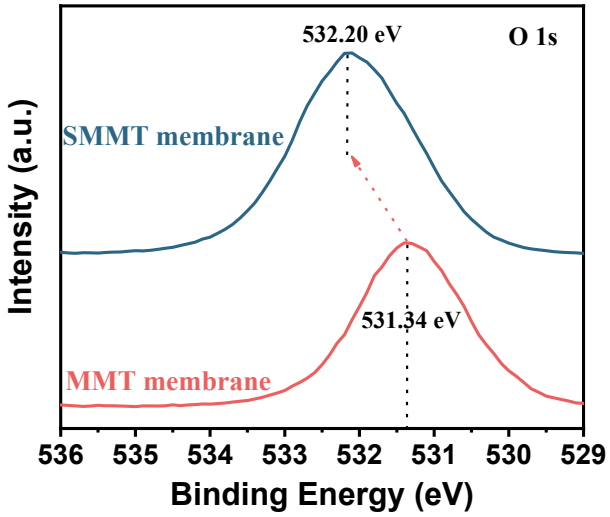

Figure S11. O 1s XPS spectra for MMT and SMMT membranes.

Note: Comparing the XPS spectra for O 1s core level of the MMT membrane, a significant blue shift was observed in the SMMT membrane, indicating the hydrogen bonding between the MMT nanosheets and the sulfonic acid groups to each other during the membrane formation process.

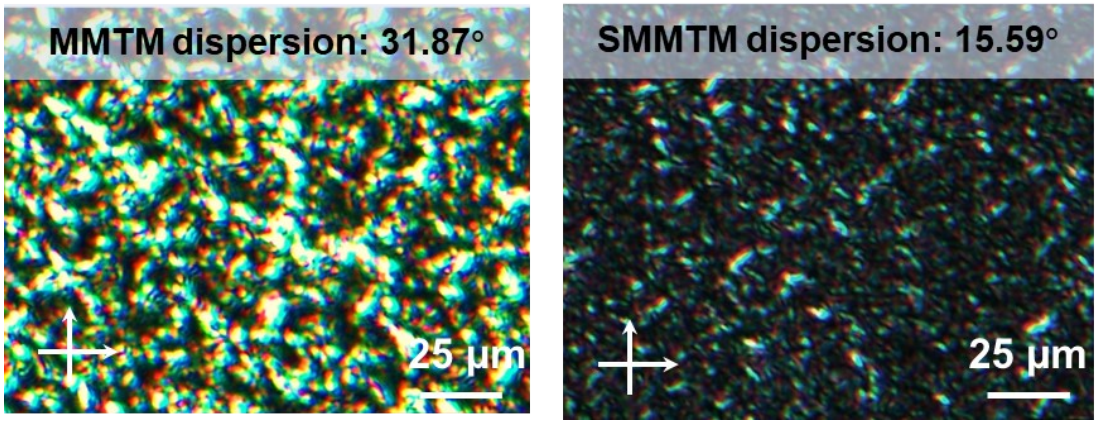

Figure S12. POM images of (a) MMT membrane and (b) SMMT membrane. Analysis of nanosheet dispersion on different membrane surfaces by Fiji ImageJ software.

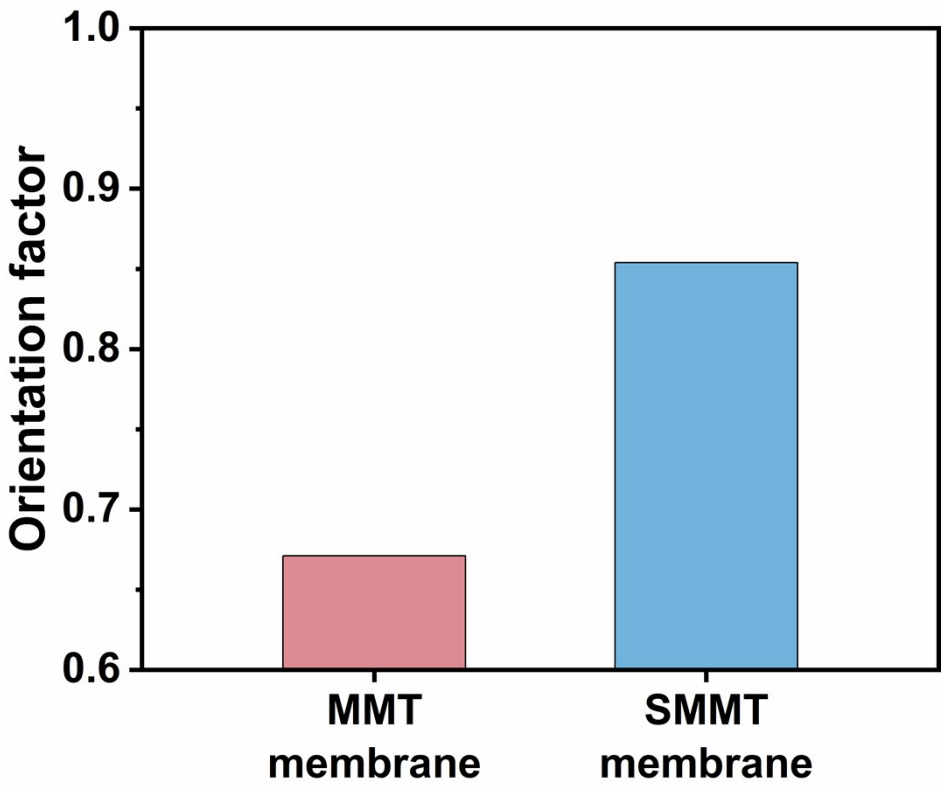

Figure S13. Comparison of orientation factors of MMT and SMMT membranes.

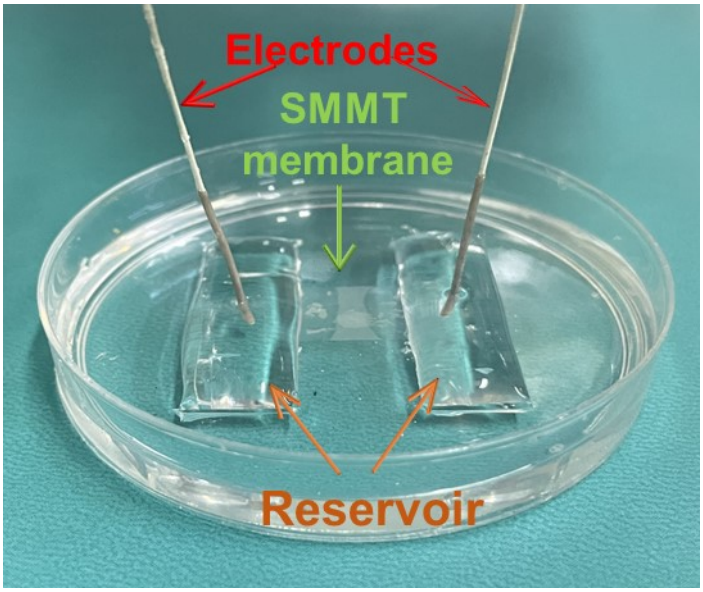

Figure S14. Photographs of the SMMT membrane embedded in PDMS.

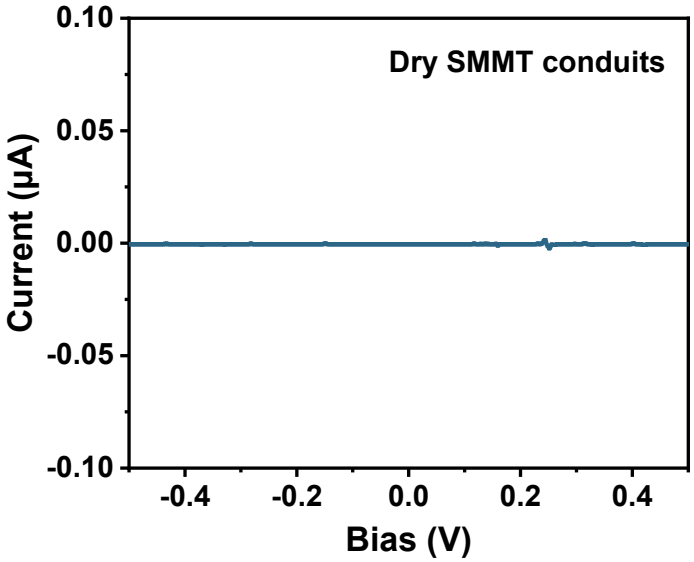

Figure S15. I-V curves obtained on dry SMMT membranes.

Note: There was no meaningful current recorded, indicating that the dry membranes were not conductive within the voltage range of -0.5-0.5 V.

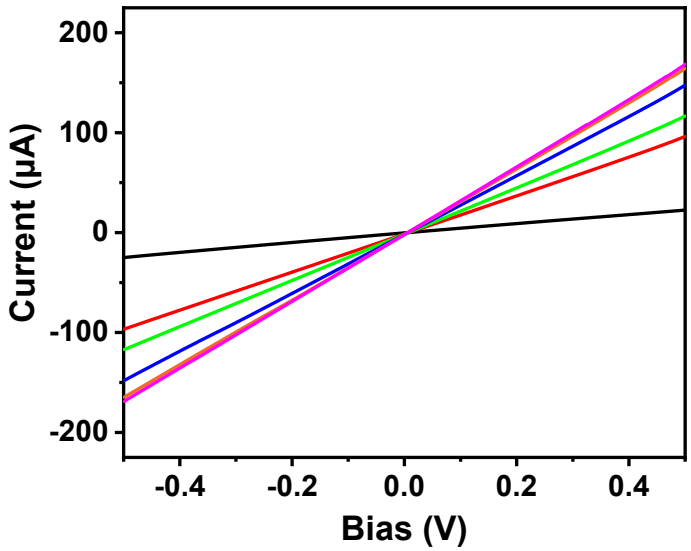

Figure S16. The representative I-V curves of the MMT membranes determined at different temperatures in 0.1 M HCl solution.

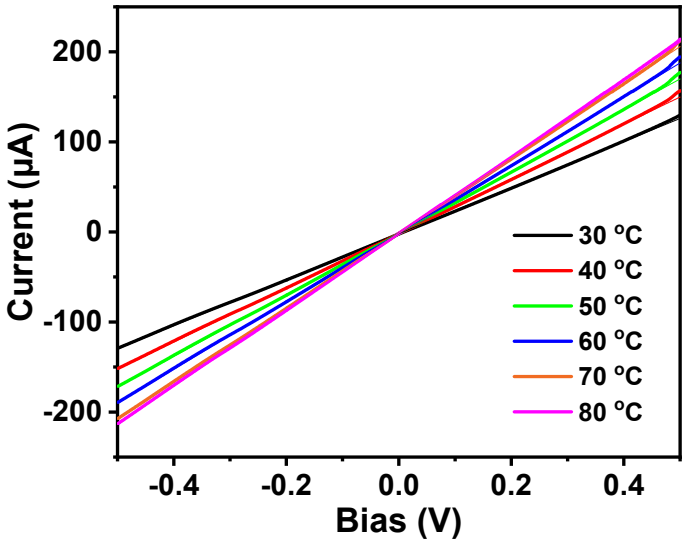

Figure S17. The representative I-V curves of the SMMT membranes determined at different temperatures in 0.1 M HCl solution.

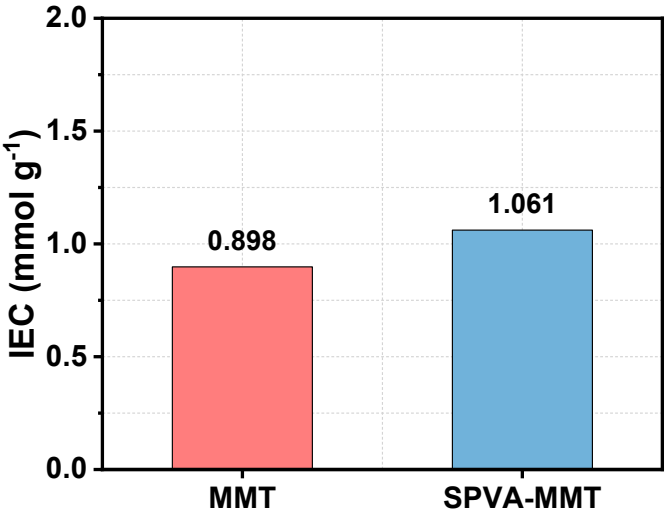

Figure S18. The IEC value of MMT and SMMT membranes.

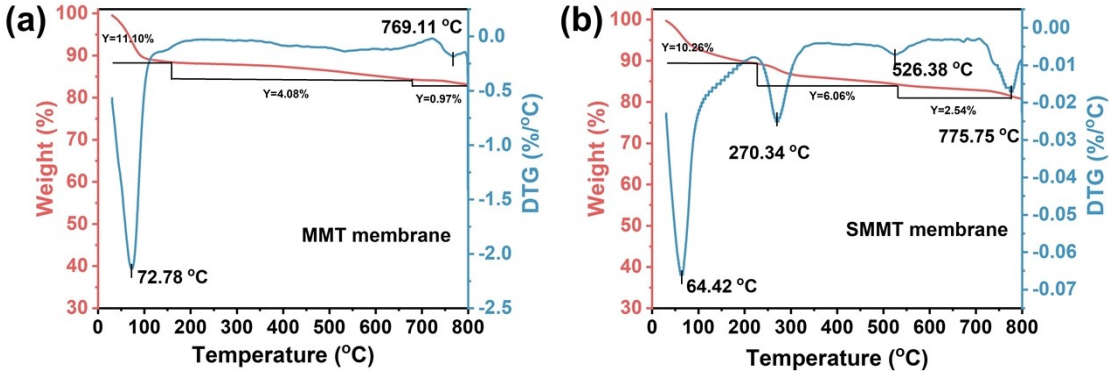

Figure S19. TGA curves of (a) MMT and (b) SMMT membranes.

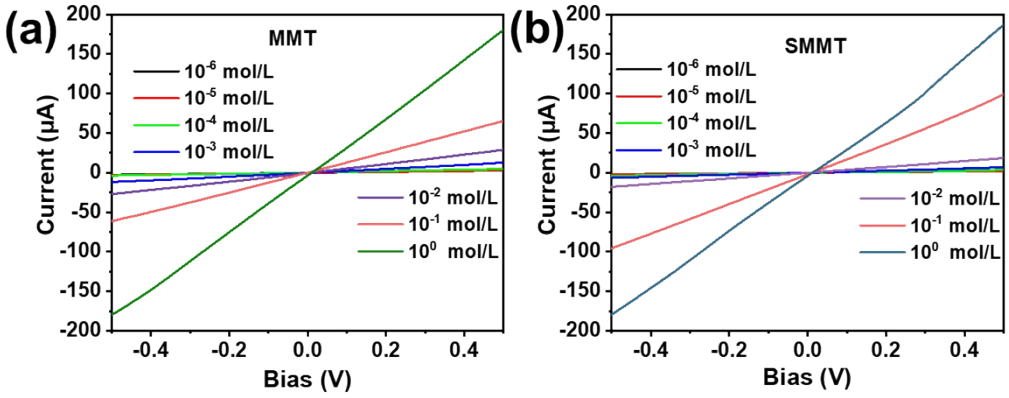

Figure S20. The representative I-V curves of MMT and SMMT membranes at HCl concentrations of 10^{-6} M ~ 10^{0} M.

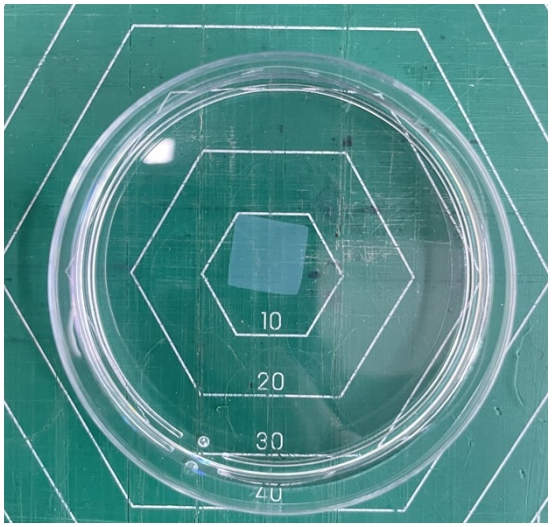

Figure S21. Photograph of the SMMT membrane immersed in 0.1 M HCl solution after 30 days.

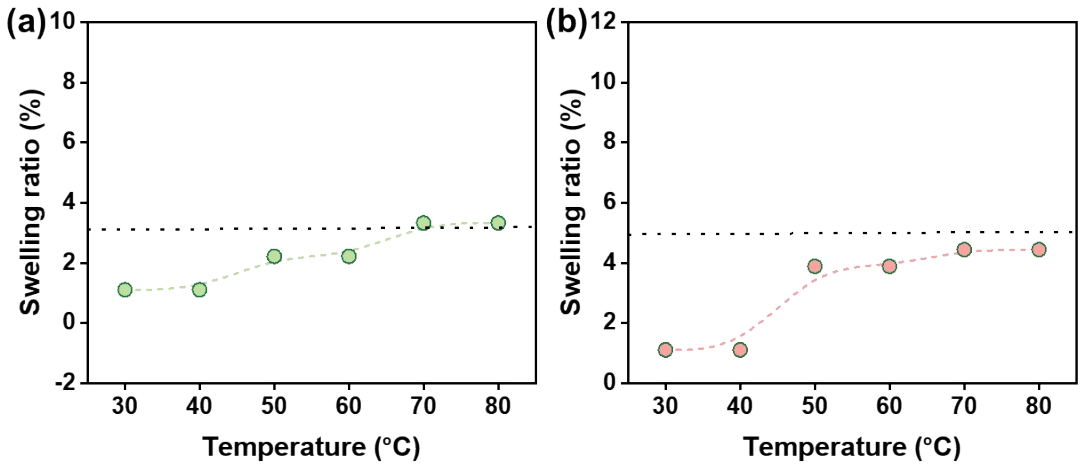

Figure S22. (a) The in-plane and (b) through-plane dimensional swelling of SMMT under different temperatures and 98% RH.

Note: To ensure that the membrane reaches equilibrium and stabilization, each experimental condition was maintained for 2 h prior to testing.

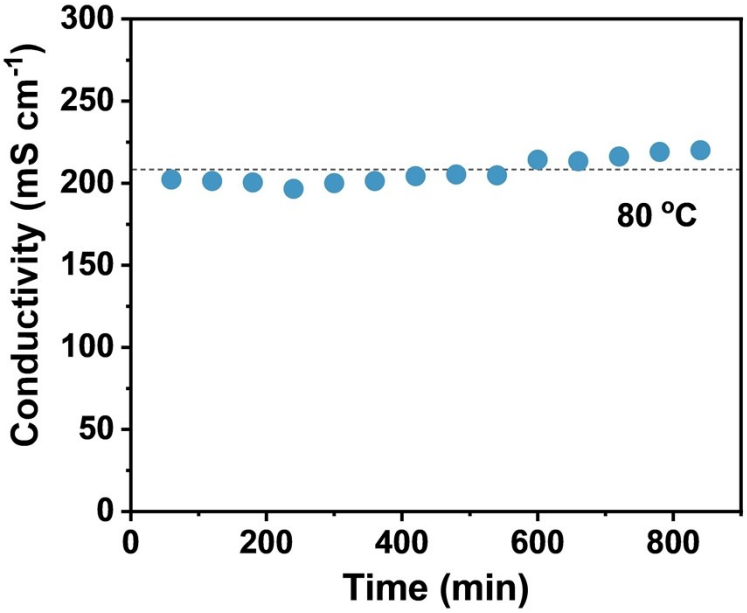

Figure S23. Proton conductivity stability of the SMMT membrane during the long-term test at 80 °C.

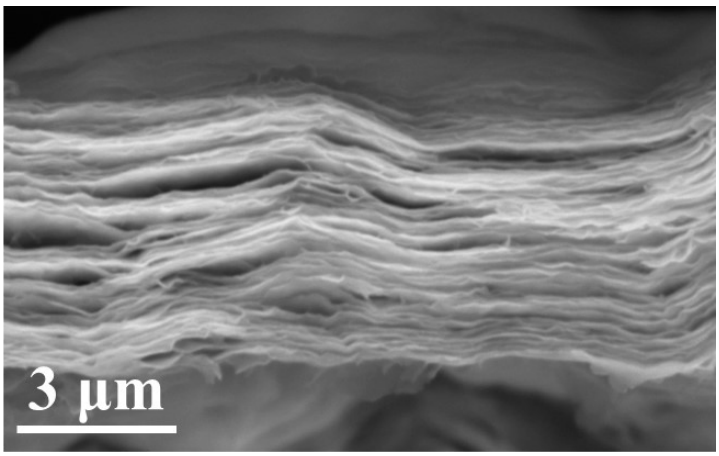

Figure S24. The SEM image of the cross-section of the SMMT membrane after long-term operation at the room temperature.

Note: The SMMT membrane remained aligned nanochannel structure after long-term operation, indicating the strong structural stability of SMMT membrane.

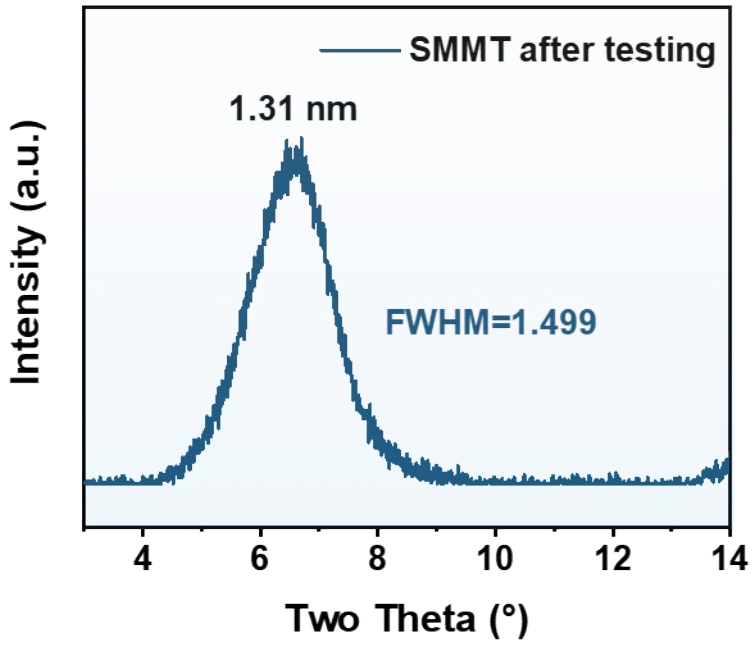

Figure S25. The XRD pattern of the SMMT membranes after long-term operation at the room temperature.

Note: The XRD characteristic peaks and FWHM of the SMMT membrane remained essentially unchanged after long-term operation, illustrating the structural stability of the SMMT membranes.

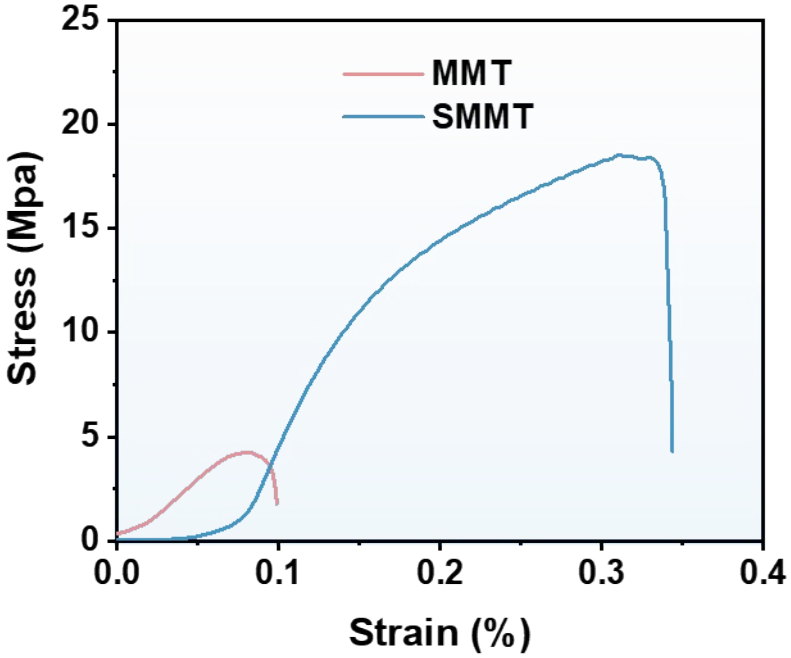

Figure S26. The stress-strain curves of MMT and SMMT membranes.

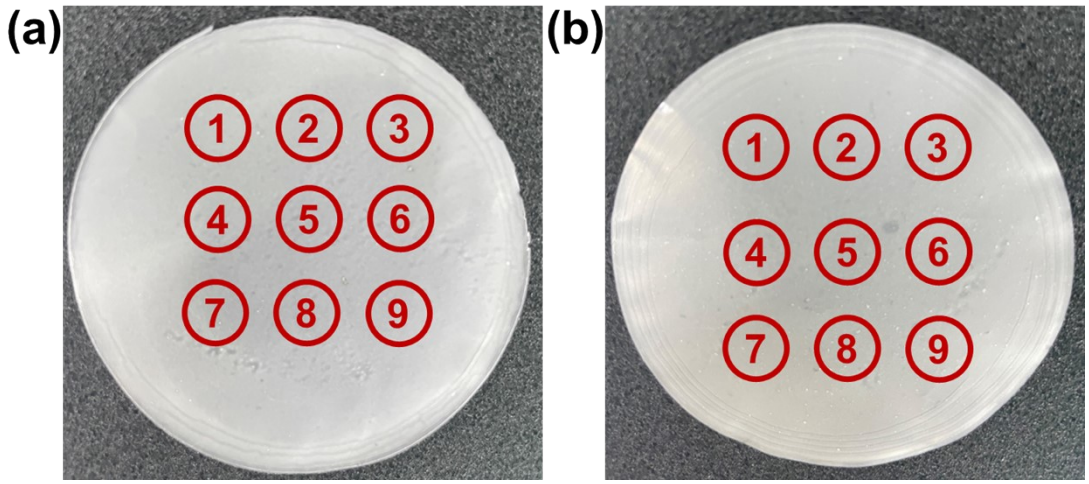

Figure S27. Photograph of selected regions from scaled-up SMMT membranes with the same preparation conditions.

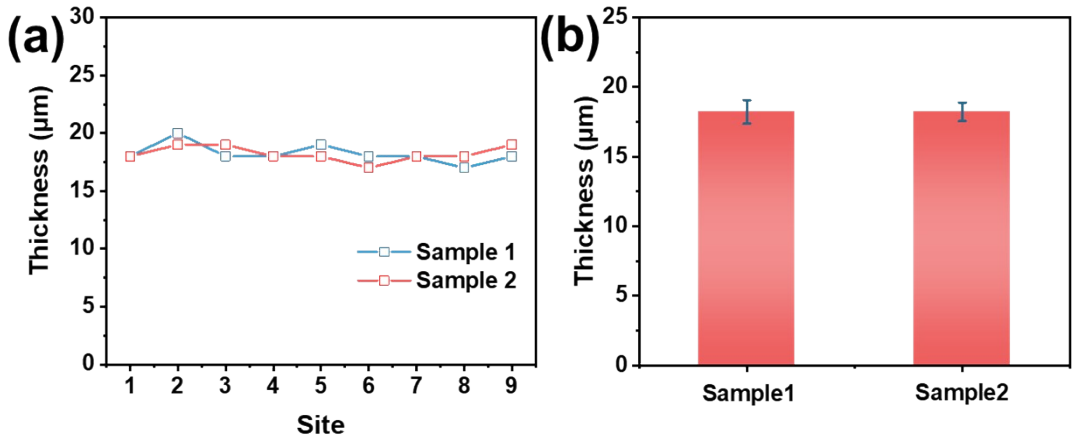

Figure S28. (a) The thickness of different sites from SMMT membranes. (b) Average thickness of different SMMT membranes. The error bars in the figure represent the standard deviations for nine measurements.

3. Supplementary tables

Table S1. Comparison of proton conductivity and *E*a of the SMMT membrane with PEMs reported in the literature.

PEMs	*E*a (KJ mol^{-1})	σ (mS cm^{-1})	References
GO-20%HA	6.75395	23	[5]
GO-15%HA	6.75395	25	
GO-10%HA	8.68365	22	
GO	9.6485	20	
CSM-X composite	8.97	35	[6]
Boron Nitride	9.6485	40	[7]
Eu-I-230	10.61335	36	[8]
Tb-I-230	13.5079	29	
SD-Tb-I	29.91035	15	
Vermiculite	18.33215	26	[9]
MIL-53/PET	19.297	110	[10]
MIL-53-NH_2/PET	31.84005	105	
SLMO	20.2618	35	[11]
SMMT	9.19	134.58	This work

Table S2. Comparison of proton conductivity of the SMMT membrane in the low (0.1 mM) and high (0.1 M) proton concentration with PEMs reported in the literature.

PEMs	σ in 0.1 M (mS cm^{-1})	σ in 0.1 mM (mS cm^{-1})	References
Boron Nitride（BN）	40	0.15	[7]
Vermiculite	26	7	[9]
PET	50	0.09	[10]
MIL-53-NH2/PET	105	0.15	
MIL-53/PET	110	0.5	
GO	20	0.6	[5]
GO-10%HA	22	0.7	
GO-20%HA	23	3.5	
GO-15%HA	25	3.7	
SMMT	117.64706	4.05882	This work

Table S3. Comparison of proton conductivity and tensile strength between the SMMT membrane with PEMs reported in the literature.

PEMs	Tensile stress (MPa)	σ (mS cm^{-1})	References
MN-A	5.4	16	[12]
C-SPEEK	21.62	17	[13]
CS/H_2SO_4@MIL-101-12	30	34	[14]
MII	30.1	17	[15]
TB-COFs	40	60	[3]
M-BC	25	90.2	[16]
SF-Nafion-1	13	130	[17]
MIV	6.25	32	[18]
Recast Nafion	15.2	69	[19]
Nafion/LSA-15	8.9	62	
Nafion/LSA-5	12.8	63	
Nafion/LSA-20	8.2	60	
SMMT	15.72	134.58	This work

4. Supplementary references

1. G. He, M. Xu, J. Zhao, S. Jiang, S. Wang, Z. Li, X. He, T. Huang, M. Cao, H. Wu, M. D. Guiver and Z. Jiang, *Adv. Mater.*, 2017, **29**, 1605898.
2. C. Zhao, P. Zhang, J. Zhou, S. Qi, Y. Yamauchi, R. Shi, R. Fang, Y. Ishida, S. Wang, A. P. Tomsia, M. Liu and L. Jiang, *Nature*, 2020, **580**, 210-215.
3. L. Zhu, P. Ye, L. Zhang, Y. Ren, J. Liu, J. Lei and L. Wang, *Small*, 2024, **20**, 2304575.
4. C. Y. Yuan, Q. Li, Y. F. Dong, Z. P. Mao, W. D. He, C. Q. Yan, Y. H. Wang and P. Cheng, *J. Polym. Res.*, 2025, **32**, 25.
5. T. J. Konch, R. K. Gogoi, A. Gogoi, K. Saha, J. Deka, K. A. Reddy and K. Raidongia, *Mater. Chem. Front.*, 2018, **2**, 1647-1654.
6. L. Zhu, H. Yang, T. Xu, L. Wang, J. Lei and C. Si, *Adv. Funct. Mater.*, 2024, **n/a**, 2419334.
7. S. Qin, D. Liu, G. Wang, D. Portehault, C. J. Garvey, Y. Gogotsi, W. Lei and Y. Chen, *J. Am. Chem. Soc.*, 2017, **139**, 6314-6320.
8. I. R. Salcedo, R. M. P. Colodrero, M. Bazaga-García, M. López-González, C. del Río, K. Xanthopoulos, K. D. Demadis, G. B. Hix, A. D. Furasova, D. Choquesillo-Lazarte, P. Olivera-Pastor and A. Cabeza, *ACS Appl. Mater. Interfaces*, 2021, **13**, 15279-15291.
9. J.-J. Shao, K. Raidongia, A. R. Koltonow and J. Huang, *Nat. Commun.*, 2015, **6**, 7602.
10. X. Li, H. Zhang, H. Yu, J. Xia, Y.-B. Zhu, H.-A. Wu, J. Hou, J. Lu, R. Ou, C. D. Easton, C. Selomulya, M. R. Hill, L. Jiang and H. Wang, *Adv. Mater.*, 2020, **32**, 2001777.
11. H. Jin, J. Li, Z. Xu, Z. Hu, K. Liu, K. Liu, J. Duan, B. Hu, L. Huang and J. Zhou, *Sci. China Mater.*, 2022, **65**, 2578-2584.
12. Y. Wang, H. Gao, W. Wu, Z. Zhou, Z. Yang, J. Wang and Y. Zou, *Nano Res.*, 2022, **15**, 3195-3203.
13. F. Sun, L.-L. Qin, J. Zhou, Y.-K. Wang, J.-Q. Rong, Y.-J. Chen, S. Ayaz, Y. U. Hai-Yin and L. Liu, *J. Membr. Sci.*, 2020, **611**, 118381.
14. X.-Y. Dong, J.-J. Li, Z. Han, P.-G. Duan, L.-K. Li and S.-Q. Zang, *J. Mater. Chem. A*, 2017, **5**, 3464-3474.
15. L. Ahmadian-Alam and H. Mahdavi, *Renewable Energy*, 2018, **126**, 630-639.
16. Y. Sui, Y. Du, H. Hu, J. Qian and X. Zhang, *J. Mater. Chem. A*, 2019, **7**, 19820-19830.
17. J. Li, K. Fan, W. Cai, L. Ma, G. Xu, S. Xu, L. Ma and H. Cheng, *J. Power Sources*, 2016, **332**, 37-41.
18. L. Ahmadian-Alam, M. Kheirmand and H. Mahdavi, *Chem. Eng. J.*, 2016, **284**, 1035-1048.
19. L. Zhu, Y. Li, J. Zhao, J. Liu, J. Lei, L. Wang and C. Huang, *Chem. Commun.*, 2021, **57**, 9288-9291.